Study of the April 20, 2007 CME-Comet Interaction Event with an MHD Model

Y. D. Jia[1], C. T. Russell[1], L. K. Jian[1], W. B. Manchester[2], O. Cohen[2], A. Vourlidas[3], K. C. Hansen[2], M. R. Combi[2], T. I. Gombosi[2]

ABSTRACT

This study examines the tail disconnection event on April 20, 2007 on comet 2P/Encke, caused by a coronal mass ejection (CME) at a heliocentric distance of 0.34 AU. During their interaction, both the CME and the comet are visible with high temporal and spatial resolution by the STEREO-A spacecraft. Previously, only current sheets or shocks have been accepted as possible reasons for comet tail disconnections, so it is puzzling that the CME caused this event. The MHD simulation presented in this work reproduces the interaction process and demonstrates how the CME triggered a tail disconnection in the April 20 event. It is found that the CME disturbs the comet with a combination of a 180° sudden rotation of the interplanetary magnetic field (IMF), followed by a 90° gradual rotation. Such an interpretation applies our understanding of solar wind-comet interactions to determine the *in situ* IMF orientation of the CME encountering Encke.

Subject headings: comets: individual (2P/Encke)—Sun: coronal mass ejections—MHD

1. Introduction

The atmosphere of a comet continuously interacts with the solar wind, which in turn varies continually in the frame of the comet. This variability makes both real and apparent changes in the appearance of cometary plasma tails. Better knowledge of such interaction processes enhances our ability to infer the *in situ* solar wind conditions from their observed behavior.

[1]IGPP, University of California, Los Angeles, CA 90095

[2]CSEM, University of Michigan, Ann Arbor, MI, 48109

[3]Solar Physics Branch, Space Science Division, Naval Research Laboratory, Washington, DC 20375

Disconnection events (DEs) are the most dramatic interactions between the solar wind and comets. During such events, the entire plasma tail is uprooted while a new tail grows, usually accompanied by the appearance and disappearance of tail rays. As summarized by Voelzke (2005), two types of solar wind structures are believed to be responsible for the onset of DEs: interplanetary shocks and heliospheric current sheets (HCS).

In recent years, a third source of tail disconnections has been observed. Coronal mass ejections (CMEs) also appear to be able to cause DEs, but how they create DEs has never been fully understood (e.g. Buffington et al. (2008); Kuchar et al. (2008)). On April 20, 2007, Heliospheric Imager-1 (HI-1) of the Sun-Earth Connection Coronal and Heliospheric Investigation (SECCHI) aboard the STEREO-A spacecraft (Howard et al. 2008) captured a DE when a CME hit comet 2P/Encke at 0.34AU. Both the traveling CME and the variation in the Encke plasma tail are visible with high spatial and temporal resolution, providing an opportunity to study the nature of such processes (Vourlidas et al. 2007). This event is hereafter called "the April 20 event".

In this letter, the interaction sequence is examined and reproduced by magnetohydrodynamic (MHD) modeling. Our result supports that the tail disconnection is caused by the flux rope structure (e.g. (Russell & Jian 2008)) embedded in the CME. The real-time interaction of a flux rope with comet Encke in our simulation explains both the unusual appearance and time evolution recorded by STEREO. Herein we attempt to reconstruct the CME from both HI-1 images and the cometary response, which together constrain the *in situ* magnetic field orientation in the CME at 0.34 AU.

2. Observations

Comet 2P/Encke is a Jupiter family comet with an orbital period of 3.3 years and a perihelion production rate of approximately $2 \sim 6 \times 10^{28}\, s^{-1}$ (Mäkinen et al. 2001; Lisse et al. 2005). On April 20, 2007, comet Encke was traveling from north to south at an orbital speed of approximately $60\, km/s$, having just passed perihelion close to the ecliptic plane (See http://ssd.jpl.nasa.gov/horizons.cgi). During the April 20 event, the STEREO-A spacecraft was in its heliocentric orbit close to the Earth. The HI-1 measures Thomson scattered light with a passband of $630 \sim 730\, nm$.

Figure 1 shows the interaction stages with images extracted from the online animation in (Vourlidas et al. 2007). The sun is to the left, while the solar wind flows to the right. The tail of comet Encke is the bright line in the center, with the head lying at the left. In each image, there is a vertical bright front and its succeeding dark region. The bright cloud

represents the sheath while the dark region is a possible flux rope. Also note that the less bright region at the left side of each images is not the end of the CME. At the time of the interaction, the CME diameter is approximately 0.14 AU along the equator and 0.21 AU along the north-south direction and its center is located at 48 R_s from the Sun. Note that these are projected quantities along the sky plane and are fairly typical for such events (e.g., (Vourlidas et al. 2000; Subramanian & Vourlidas 2007)). If we assume self-similar expansion, we estimate that the structure was about 0.6 R_s in diameter when it erupted. The larger size along the normal to the equator implies that the CME is 'pancaking' as has been predicted by several models (e.g., (Riley & Crooker 2004)). These measurements relate to the outer envelope of the CME which includes overlying streamer material and likely overestimates the actual size of the magnetic fluxrope. Since this is generally considered to be the dark void in white light CMEs, we estimate a fluxrope size of 0.06 AU by measuring the dark region behind the bright front. This diameter is consistent with the diameter estimated from the time elapsed for the dark region to pass the comet with a speed of $500 km/s$.

The diameter, as estimated above, is the lower limit of this flux rope but is significantly smaller than the average diameter at this heliocentric distance (e.g., (Lepping & Wu 2007; Jian et al. 2008)). However, the size of the CME is consistent with similar measurements in the LASCO coronagraphs. Besides, our calculations are based on direct measurements of CME features while in-situ estimates are based on model fits to the magnetic data and could suffer significant uncertainties. On the other hand, numerous small scale fluxropes have been detected with the STEREO in-situ instruments (Kilpua1 et al. 2009). Therefore, our estimates for the fluxrope size are reasonable and can use them in the simulations with confidence.

At 18:10 UT, the leading side of the CME flux rope is $1\times10^6 km$ downstream of the comet head. At 18:50 UT, the comet tail is elongated while starting to break away from the head. At 19:30 UT, the comet head is engulfed in the flux rope region of the CME, while the tail is completely disconnected. At 20:10 UT, the gap between the disconnected tail and the comet head equals over three million kilometers.

Both the slow solar wind and the interplanetary magnetic field (IMF) were in the radial direction. The projected CME speed is about $500\, km/s$. The dynamic pressure changed less than 20% due to the CME. Although recognizable in the images, the density variation in the CME is <1%, so this DE was not caused by pressure effects Vourlidas et al. (2007). This event is puzzling for the following reasons:

First, this event appears to be different from past events. There is a long gap developed between the old tail and the end of the new tail. In addition, this DE is accompanied with tail elongation with no tail rays.

Second, this DE must have been caused by a mechanism other than a HCS crossing or shock impact, because there were neither HCS crossings nor shocks seen in the HI images. In this study we discuss how the flux rope of the CME could have caused the tail disconnection.

In the top panel of Figure 1, the CME front has caused a kink in the comet tail three million kilometers from its head. Although this kink is not modeled in our study, it does suggest that the disconnection is not caused by the CME front. The comet tail is aligned in the solar wind flow direction, so the CME encounters the comet head before it reaches the tail. At 18:50 UT, the DE becomes visible while the comet head has been in the flux rope for an hour. This scenario is consistent with the appearance of a DE caused by a 180° rotation in the IMF, with the observing line of sight perpendicular to the IMF plane (Jia et al. 2007, panel b, Figure 4). At 19:30 UT and 20:10 UT in Figure 1, the new tail appears consistent with the appearance of shortened comet tails when the observer looks through the thin direction of the current sheet (Russell et al. 1991).

3. MHD Model

In this study we use the Block Adaptive Tree Solar-wind Roe Upwind Scheme (BATS-R-US), a 3-D global MHD numerical code (Powell et al. 1999), and the Space Weather Modeling Framework (SWMF) that employs BATS-R-US for several of the coupled physical domain modules (Tóth et al. 2005).

Here, the solar corona and inner heliosphere models (based on BATS-R-US) are run with the SWMF code to predict the ambient solar wind condition at 0.34 AU (Cohen et al. 2007). The estimated IMF magnitude is 20 nT, the density is 20 amu/cm^3, the velocity is 440 km/s and the temperature is $3 \times 10^5\, K$. Such a solar wind condition is adopted as the outer boundary for the comet code.

A previous version of the BATS-R-US comet code was used for a time-dependent generalized DE study with HCS crossings (Jia et al. 2007). In this study the same code is applied to simulate the time evolution as shown in next section. The x-axis points along the solar wind flow direction, z-axis points north, and the y-axis completes the right-hand system. The calculation domain is $2.4 \times 0.4 \times 0.4$ in unit of $10^6\, km$, with finest resolution of 25 km in the cometary contact surface region, and a resolution of 800 km in the cometary tail.

For simplicity, both the radial component of the background IMF and the temperature variations in the CME are neglected. The CME structure is represented by a simplified flux rope that is $5.4{\times}10^6\, km$ across. This value is smaller than the estimated size of $9{\times}10^6\, km$, to qualitatively simulate the shorter path that the comet travels in the CME, because in

this event the comet interacts with the side or even the leg of the fluxrope Vourlidas et al. (2007). The axis of the flux rope is in the y direction. The density and velocity variations in the CME are neglected. In addition, we assume that comet Encke crossed the axis of the CME. The dimensions of the bow wave of comet Encke are estimated to be less than 0.2 $\times 10^6\,km$ (the subsolar distance is $5 \times 10^4\,km$), which is orders of magnitude smaller than the diameter of the flux rope, of which the curvature of field lines is negligible. Consequently, the interaction process is modeled simply as the effect of the rotation of the IMF vector. At initial state, the function of the magnetic field is:

$$B_x = 0\,nT$$

$$B_y = \begin{cases} 0 & +\infty \geqslant x \geqslant -0.85 \\ 20sin\left(\frac{\frac{\pi}{2}(x+0.85)}{(-3.55+0.85)}\right) & -0.85 > x > -3.55 \\ 20 & else \end{cases}$$

$$B_z = \begin{cases} 20 & +\infty \geqslant x \geqslant -0.4 \\ -20 & -0.4 > x \geqslant -0.85 \\ 20cos\left(\frac{\frac{\pi}{2}(x+0.85)}{-3.55+0.85}\right) & -0.85 > x > -3.55 \\ 0 & else \end{cases},$$

where x is the x-coordinate in unit of $10^6 km$, B is in unit of nT. The parameters, 0.4 indicates the upstream boundary of our simulation box at $-0.4 \times 10^6 km$. At 15:45 UT, the front current sheet is located at $-0.85 \times 10^6 km$, with a thickness of $0.35 \times 10^6 km$. Thus the center of the flux rope with a radius of $2.7 \times 10^6 km$ is at $-3.55 \times 10^6 km$. These parameters are selected to reproduce the general dynamics, while for a future work that compares the timing of this evolution, a more accurate set of parameters need to be tested.

4. Model Results

The model calculation of the interaction process between this CME and the comet is shown in 2-D projections of Figure 2. The color contours of plasma density show the location of the bow shock and tail. The black lines represent magnetic field lines. Left panels show the meridional plane, while right panels show the ecliptic plane. Please note that these volume densities shown in 2-D slices are not yet directly comparable to the integrated column densities in the HI images.

At 16:10 UT, the front of the flux rope (marked by the dashed vertical white lines) is at $-10^5\,km$, in front of the comet bow shock. The IMF is in the x-z plane so the tail appears thinner in this plane, and wider in the x-y plane. The comet appears similar to its initial state.

At 16:30 UT, marked by the white dashed lines, the interface of reversed field lines has formed a cone centering at the comet head. In the x-y plane, the axial component in the flux rope starts to increase behind the front, as marked by the black field lines to the left of the white dashed line. The field to the right of the white line is the old IMF pointing northward. The comet tail appears stretched in both slices. After this, the white dashed lines in panels a and b continue to fold toward the tail as this stretched interface propagates downstream.

At 17:40 UT, the tip of the interface between the reversed field lines has propagated to 400,000km, while the axis of the flux rope has entered the upstream boundary of the simulation domain (not shown). Magnetic reconnection in the tail has generated a density pileup region, which appear as the trailing head of the disconnected tail, as studied by Jia et al. (2007). At this moment the pile up region has propagated to 300,000 km, as marked by the density increase surrounded by the field line on the right. To the left of the density pile-up, a new tail starts to grow. This new tail becomes wider in the x-z plane and thinner in the x-y plane, as a consequence of field rotation in the IMF. The field to the left of the white lines has both y and z components. The old field lines pointing northward are confined in the tail to the right of the white lines. Better interpretation of the detailed evolution requires higher resolution and resistive MHD, or Hall MHD that treats the reconnection in a more realistic way.

At 18:30 UT, the axis of the flux rope is significantly bent, as marked by the red dotted line in the left panel. At the top boundary, the axis of the flux rope has passed through the shown region. Along the x-axis, the center of the flux rope has only propagated to the inner coma, while the front of the flux rope has also passed through the shown region. The IMF along this red line is primarily in the y direction (zxis component), while those to the right of the red line are rotating from the y direction to the z direction as they leave the red line. The red line in the right panel marks the interface of the field lines with the same orientation. This stretched red line suggests that the highly draped field lines significantly affects the force balance in the interaction process, and thus controls the evolution speed of this process. In the next step for a study to match the observation in real-time, the actual structure in the CME field need to be considered.

The density pile-up is at 500,000 km, as marked by the right-most field lines. To the left of the density pile-up, the developing new tail appears wider in the x-z plane and thinner in the x-y plane, consistent with the result of a 90° field rotation.

The column-integrated density contours measured along the y-direction are shown in Figure 3. The head of a disconnected tail has propagated to x=1.1×10^6 kilometers, while a short new tail is formed and stays short. The complete evolution process is available as an MPEG animation in the electronic edition of the *Astrophysical Journal*. Between 16:00 UT

and 17:20 UT, the length of the tail keeps growing, until the far tail becomes too weak to be visible. These earlier phases resembles the top image in Figure 1, where the comet tail is stretched but not separated. At 16:40 UT, the density pile-up starts to form at 50,000 km. At 17:00 UT, this region appears separated from the head and propagated to 70,000 km. The separation is only visible from the decrease in column density contours, but not directly observable yet, because it still overlaps with the new tail. At 17:20 UT, the pile-up is at 120,000 km, while the tail is stretched to its maximum length. From 17:40 UT to 18:00 UT, the density increase is at 200,000 km, while the brightness of the new tail close to the density increase is still higher than the old tail.

At 18:20 UT, the new tail appears short while the density increase is at 500,000km, separated from the old tail. After 18:40 UT, the new tail stays the same length, which is shorter than the one at 18:20 UT. The density increase, as the trailing head of the disconnected tail, propagates from 600,000 km to $1.1 \times 10^6\, km$ from 18:40 UT to 19:40 UT, resembling the phase between 18:10 UT and 19:30 UT, as shown in the two middle images of Figure 1. Afterward, the tail remains short while the old tail recesses, resembling the two lower panels in Figure 1. The simulation can be improved with a larger calculation domain and higher resolution in the tail to simulate the complete process, with an extension of $10 \times 10^6\, km$, and a two-species code to track the heavy ions to achieve a higher contrast ratio to better observe the tails. Even with its present limitations, the comparison between this modeled time sequence and the STEREO images show sufficiently similar evolution to support our interpretation.

For comparison, both a test case with only a 180° IMF sudden rotation and a case with 90° gradual rotation in 1.5 hours were studied. The 180° case produces a DE with a similar evolution speed, although not visible along the y-axis. The 90° case does not produce a DE. These two cases is comparable with case 1 and case 2 for a Halley-sized comet (35 times more gas production and thus evolves slower) presented by Jia et al. (2007).

The production rate of comet Encke used in the simulation above is the lower limit of its perihelion value during its past 4 perihelion passes. A case with its upper limit, 6×10^{28} was also studied (not shown here). In the upper limit case, the evolution exhibited similar processes, but with a stronger brightness and slower pace. Development of Hall MHD or resistive MHD models for such interactions, plus the analysis of more events, is expected to better reproduce the reconnection rate and to better address the evolution speed.

5. Discussion

In summary, the MHD simulation produces magnetic reconnection in the comet tail and provides an answer to how the CME triggered a DE in the April 20 event. The comet tail evolution results from a combination of a 180° IMF sudden rotation that causes front-side and then tail-side magnetic reconnection, with a 90° gradual rotation that reduces the number of cometary ions along the line of sight. Such an interpretation applies our understanding of solar wind-comet interactions to better constrain the *in situ* IMF orientation of this CME at 0.34 AU.

Compared with the HI-1 observation, there are still differences in detail from our idealized simulation, suggesting our numerical model should be improved. In particular, instead of a single species comet model, a two-species model that tracks both the solar wind ions and the cometary heavy ions is needed to better reveal the column density of cometary ions.

The modeled evolution pace of this DE is slower than observed. In addition to the limitation of ideal MHD, there are three possible reasons that lead to this difference. First, the comet may not pass the axis of the CME, indicating an uncertainty in the length of the path in the flux rope than assumed. In addition, the comet passed through the flank of the flux rope rather than the axis (Vourlidas et al. 2007). The asymmetry in the flux rope may affect the magnetic pressure during the evolution. Second, the real 3-D field and plasma conditions of the flux rope may provide stronger acceleration force to the disconnected tail. In this case, the curvature of azimuthal field may cause stronger tension force while interacting with the cometary structures. Lastly, a stronger IMF, or more complex field and plasma fluctuations in the flux rope may speed up this process.

The IMF conditions behind the axis of the flux rope are not examined in this model. From this disconnection event, the cometary tail grows longer after the CME has passed, indicating that the IMF is back in the x-z direction.

It should be noted that this study is limited to one type of CME-comet interaction mechanism. Clearly, CME-comet interactions involve several different physical processes, and the observed DEs are formed in a variety of ways. We need to gather more *in situ* data at the times of cometary tail disconnections to understand fully the range of interaction leading to these disconnection events.

REFERENCES

Buffington, A., Bisi, M. M., Clover, J. M., Hick, P. P., Jackson, B. V., & Kuchar, T. A.

2008, ApJ, 677, 798

Cohen, O., et al. 2007, ApJ, 654, L163

Howard, R. A., et al. 2008, Space Science Reviews, 136, 67

Jia, Y.-D., Combi, M. R., Hansen, K. C., & Gombosi, T. I. 2007, J. Geophys. Res., 112, 05223

Jian, L. K., Russell, C. T., Luhmann, J. G., Skoug, R. M., & Steinberg, J. T. 2008, Sol. Phys., 249, 85

Kilpua1, E. K. J., et al. 2009, Solar Phys., 254, 325

Kuchar, T. A., et al. 2008, J. Geophys. Res., 113, A04101

Lepping, R. P., & Wu, C.-C. 2007, Journal of Geophysical Research (Space Physics), 112, 10103

Lisse, C. M., et al. 2005, ApJ, 635, 1329

Mäkinen, J. T. T., Silén, J., Schmidt, W., Kyrölä, E., Summanen, T., Bertaux, J.-L., Quémerais, E., & Lallement, R. 2001, Icarus, 152, 268

Powell, K. G., Roe, P. L., Linde, T. J., Gombosi, T. I., & Zeeuw, D. L. D. 1999, J. Comput. Phys., 154, 284

Riley, P., & Crooker, N. U. 2004, ApJ, 600, 1035

Russell, C. T., & Jian, L. 2008, Advances in Space Research, 41, 1177

Russell, C. T., Le, G., Luhmann, J. G., & Fedder, J. A. 1991, Washington DC American Geophysical Union Geophysical Monograph Series, 61, 65

Subramanian, P., & Vourlidas, A. 2007, A&A, 467, 685

Tóth, G., et al. 2005, J. Geophys. Res., 110, 12226

Voelzke, M. R. 2005, Earth Moon and Planets, 97, 399

Vourlidas, A., Davis, C. J., Eyles, C. J., Crothers, S. R., Harrison, R. A., Howard, R. A., Moses, J. D., & Socker, D. G. 2007, ApJ, 668, L79

Vourlidas, A., Subramanian, P., Dere, K. P., & Howard, R. A. 2000, ApJ, 534, 456

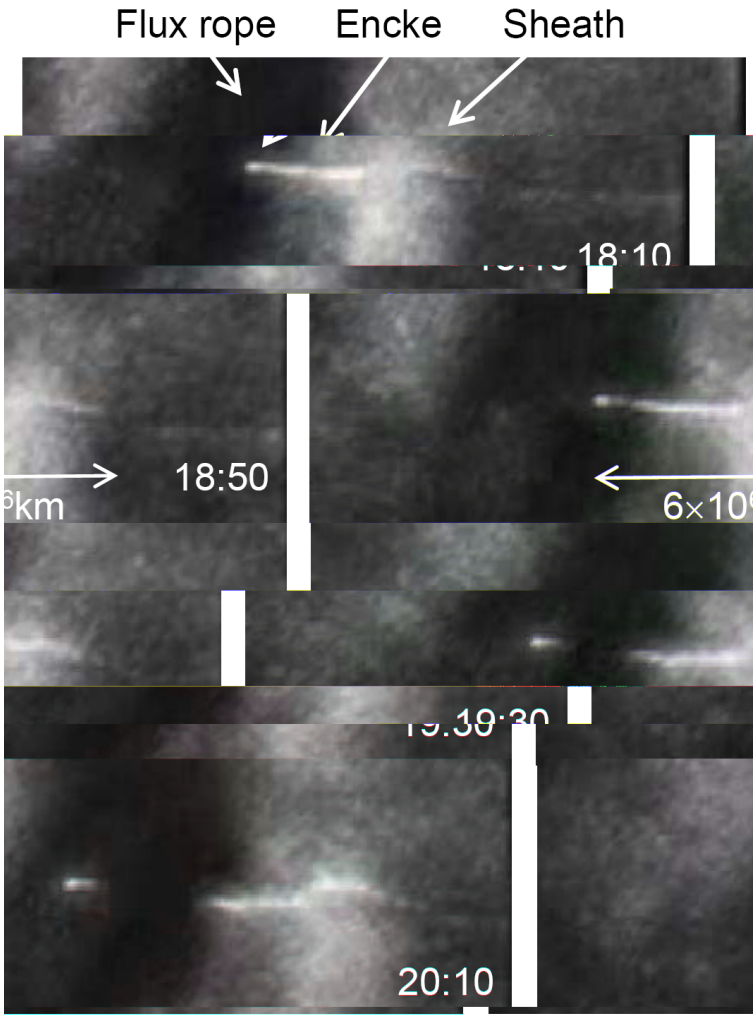

Fig. 1.— Time sequence of the CME-comet interaction process observed by the STEREO A HI-1. Brightness represents relative density. Solar wind comes from the left, while comet Encke and its tail is at the center pointing to the right. As marked by the arrows, the bright cloud shows the front sheath of the CME, while the dark region shows the flux rope. Images extracted and enhanced from online material by Vourlidas et al. (2007).

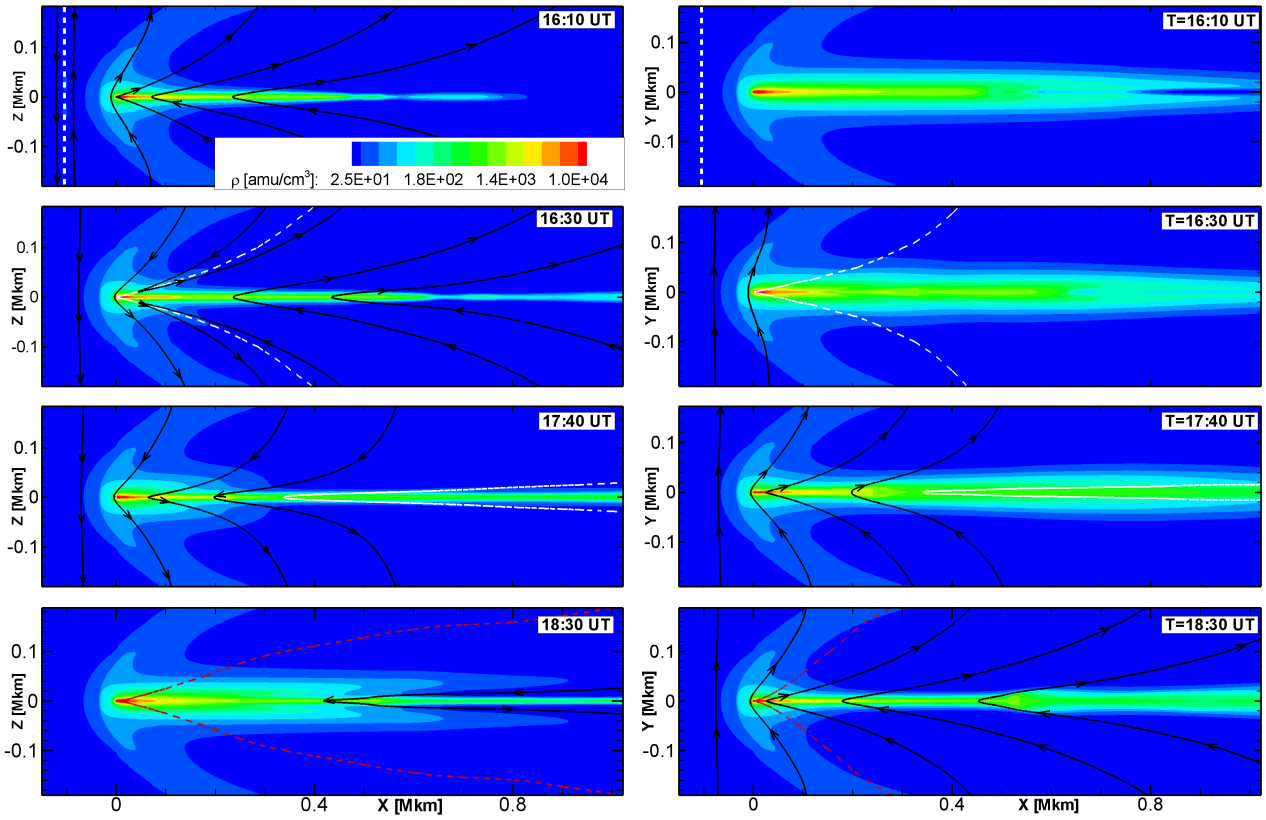

Fig. 2.— The time evolution of the disconnection event in 2-D slices. Color contours represent plasma density showing the bow shock and tail. The black lines represent magnetic field lines. White dotted lines show the current sheets, while red dashed lines show the location of the flux rope axis. Left panels show the meridional plane, while panels on the right show the ecliptic plane.

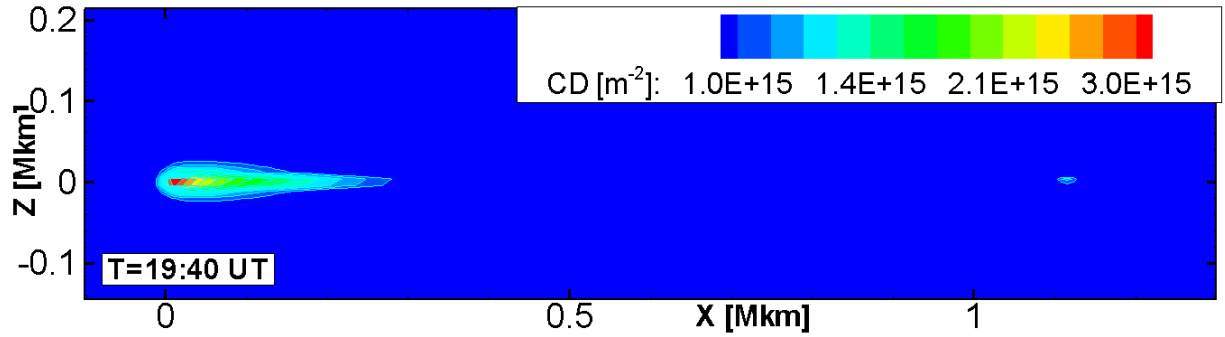

Fig. 3.— The column density along the y-axis at 2:30h. This figure is a still image from an MPEG animation of the interaction process available in the electronic edition.